System of two Hamilton-Jacobi equations for complex-valued travel time

Luděk Klimeš
Department of Geophysics, Faculty of Mathematics and Physics, Charles University, Ke Karlovu 3, 121 16 Praha 2, Czech Republic, http://sw3d.cz/staff/klimes.htm

Summary

Since waves propagate in real space and since the material properties are known in real space only, we cannot calculate complex–valued rays. In real space, the eikonal equation for complex–valued travel time represents the system of two Hamilton–Jacobi equations for the real and imaginary parts of the complex–valued travel time. Unfortunately, the solution of this system of Hamilton–Jacobi equations does not propagate along rays, and has to be solved by more global numerical methods.

We propose to consider a system of surfaces and to calculate the complex–valued travel time from one surface to the subsequent surface numerically. This method may be suitable for application to wavefront tracing.

We present three simple examples of the numerical calculation of the complex–valued travel time, and compare their results with the analytical solutions.

Keywords

Wave propagation, attenuation, eikonal equation, complex–valued travel time, system of Hamilton–Jacobi equations.

In: Seismic Waves in Complex 3–D Structures, Report 19 (Department of Geophysics, Charles University, Prague, 2009), pp. 157–171

1. Introduction

Eikonal equation in a non–attenuating medium may be solved in terms of the real–valued travel time or in terms of the complex–valued travel time, depending on the initial conditions. One of reasons for complex–valued initial conditions is representation of the initial amplitude in terms of the initial imaginary part of travel time. It is well known that the representation of amplitude variations in terms of complex–valued travel time increases the accuracy of the ray methods. For example, if we represent the initial envelope of a Gaussian beam by the imaginary part of travel time, we usually obtain a reasonable solution. If we represent the initial envelope of a Gaussian beam by amplitude, the evolution of the envelope resulting from the transport equation is incorrect (Kravtsov, personal communication).

Eikonal equation in an attenuating medium must be solved in terms of the complex–valued travel time.

Solution of the complex–valued eikonal equation for complex–valued travel time by the Hamilton's (1937) equations of rays would require complex–valued rays. Since waves propagate in real space and since the material properties are known in real space only, we cannot calculate complex–valued rays. In real space, the eikonal equation for complex–valued travel time represents the system of two Hamilton–Jacobi equations for the real and imaginary parts of the complex–valued travel time. Unfortunately, the solution of this system of Hamilton–Jacobi equations does not propagate along rays, and has to be solved by more global numerical methods. Two approximate methods for solving the complex–valued eikonal equation for complex–valued travel time in real space were proposed by Suchy (1972, secs. 4, 5).

In this paper, we propose to consider a system of surfaces and to calculate the complex–valued travel time from one surface to the subsequent surface numerically. This method may be suitable for application to wavefront tracing (Vinje, Iversen & Gjøystdal, 1993; Vinje et al., 1996), but poses a problem how to modify wavefronts in vicinities of caustics in order to obtain a reasonable system of surfaces for calculating the complex–valued travel time.

It is obvious that the solution of the system of Hamilton–Jacobi equations for complex–valued travel time is a long–term problem. It will require to design new numerical algorithms, to study the stability and accuracy of these algorithms, and to estimate the propagation of numerical errors in these algorithms.

Lower–case roman indices $a, b, ... = 1, 2, 3$ correspond to three spatial coordinates. Upper–case roman indices index the action functions and the Hamilton–Jacobi equations. Lower–case greek subscripts index the points along the chosen surfaces. The Einstein summation over repetitive indices is used throughout the paper.

2. General system of Hamilton–Jacobi equations

We consider system

$$H^I\big(x^k, S_{J,j}(x^m)\big) = 0 \quad , \qquad I = 1, 2, ..., N \quad , \qquad J = 1, 2, ..., N \tag{1}$$

of N Hamilton–Jacobi equations for N action functions $S_1(x^m)$, $S_2(x^m)$, ..., $S_N(x^m)$. Here we use notation

$$S_{J,i} = \frac{\partial S_J}{\partial x^i} \tag{2}$$

for partial derivatives with respect to spatial coordinates x^i. For the partial derivatives of Hamiltonian function $H^I(x^i, p_{1j}, p_{2k}, ..., p_{Nn})$ with respect to components p_{Jk} of slowness vectors, we shall use notation

$$H^{I,Jj} = \frac{\partial H^I}{\partial p_{Jj}} \quad . \tag{3}$$

For example,

$$H^{I,Jj}_{,l} = \frac{\partial^3 H^I}{\partial p_{Jj} \partial p_{Kk} \partial x^l} \quad . \tag{4}$$

2.1. Propagation equations for action gradients

Differentiating equations (1) with respect to spatial coordinates x^i, we obtain equations

$$H^{I,Jj} S_{J,ji} + H^I_{,i} = 0 \quad . \tag{5}$$

2.1.1. Single Hamilton–Jacobi equation

For a single Hamilton–Jacobi equation, equation (5) reads

$$H^{,j} S_{,ji} + H_{,i} = 0 \quad , \tag{6}$$

which means that if we change the position by $\mathrm{d}x^j = H^{,j}\mathrm{d}\gamma_3$, slowness vector $p_i = S_{,i}$ changes by $\mathrm{d}p_i = -H_{,i}\,\mathrm{d}\gamma_3$. This property may be expressed in the form of well–known Hamilton's equations

$$\frac{\mathrm{d}x^i}{\mathrm{d}\gamma_3} = H^{,i} \quad , \tag{7}$$

$$\frac{\mathrm{d}p_i}{\mathrm{d}\gamma_3} = -H_{,i} \quad , \tag{8}$$

and used for calculation of action S.

2.1.2. System of two Hamilton–Jacobi equations

For the system of 2 Hamilton–Jacobi equations, (5) reads

$$H^{1,1j} S_{1,ji} + H^{1,2j} S_{2,ji} + H^1_{,i} = 0 \quad , \tag{9}$$

$$H^{2,1j} S_{1,ji} + H^{2,2j} S_{2,ji} + H^2_{,i} = 0 \quad . \tag{10}$$

We cannot say how slowness vector $p_{1i} = S_{1,i}$ changes in the direction of vector $H^{1,1j}$ unless we know how slowness vector $p_{2i} = S_{2,i}$ changes in the direction of vector $H^{1,2j}$, etc.

2.2. Solving a general system of Hamilton–Jacobi equations

For the system of N Hamilton–Jacobi equations, we have $N \times N$ vectors $H^{I,Jj}$, analogous to the ray–velocity vector, at each spatial point, but have no ray along which we could calculate the solution.

We shall try to solve the system of Hamilton–Jacobi equations by a method similar to wavefront tracing. We shall consider a system of surfaces and calculate the action functions from one surface to the subsequent surface.

The applicability and accuracy of this method will obviously depend on the selection of these surfaces in the first place. In the second place, the applicability and accuracy of the method will depend on the selection of discrete points at the surfaces for sampling the action functions. Note that the system of surfaces for calculating the action functions should respect the multi–valued nature of action functions, which implies that the selection of the surfaces will constitute a very difficult task.

We assume that the values $S_I(x_\alpha^m)$ of action functions are known at given discrete points x_α^m situated at a given surface. For more accurate methods, we assume to know also the values of the derivatives of action functions along the surface. We then calculate these values at corresponding points $\widetilde{x}_\alpha^m$ situated at a close subsequent surface.

At each point x_α^m, we define vector

$$t_3^i = (\widetilde{x}_\alpha^i - x_\alpha^i)/h_3 \tag{11}$$

leading from point x_α^m at the given surface to corresponding point $\widetilde{x}_\alpha^m$ at the subsequent surface. Here h_3 is the optional step in the independent parameter γ_3 parametrizing the system of surfaces. We may set

$$h_3 = 1 \quad . \tag{12}$$

At each point x_α^m, we denote two vectors tangent to the given surface by t_1^i and t_2^i. Vectors t_1^i and t_2^i can be determined from the positions of several given points situated close to point x_α^m at the given surface so as to optimize the finite–difference scheme for determination of the first–order derivatives in the directions of these vectors. We shall refer to the derivatives in the directions of vectors t_1^i and t_2^i as the *lateral derivatives*.

We introduce covariant vectors $\hat{t}_i^1$, $\hat{t}_i^2$ and $\hat{t}_i^3$ biorthonormal to t_1^i, t_2^i and t_3^i,

$$\hat{t}_i^a \, t_a^k = \delta_i^k \quad . \tag{13}$$

2.2.1 Calculation of action functions only

We assume that the values $S_I(x_\alpha^m)$ of action functions are known at given discrete points x_α^m situated at a given surface. We then calculate the values of action functions at corresponding points $\widetilde{x}_\alpha^m$ situated at the subsequent surface by a numerical method similar to one of the methods proposed by Vidale (1988).

We define first–order action derivatives

$$T_{Ia} = S_{I,j} \, t_a^j \tag{14}$$

covariantly transformed to vectors t_a^j. Then

$$S_{I,j} = \hat{t}_j^a \, T_{Ia} \quad , \tag{15}$$

and system (1) of Hamilton–Jacobi equations reads

$$\boxed{H^I\big(x_\alpha^k, \hat{t}_j^a(x_\alpha^m) T_{Ja}(x_\alpha^m)\big) = 0 \quad .} \tag{16}$$

We calculate the lateral first–order derivatives T_{I1} and T_{I2} of S_I along the given surface by finite differences. Note that calculating lateral derivatives T_{I1} and T_{I2} may represent a considerable problem in vicinities of caustics, where the second–order derivatives of S_I are very large.

For given T_{I1} and T_{I2}, (16) represents the system of N nonlinear equations for N unknowns T_{I3}. By solving this system, we obtain derivatives T_{I3} of S_I along the path of integration at point x_α^m. We can thus calculate for given $S_I(x_\alpha^m)$ their derivatives $\frac{\mathrm{d}S_I}{\mathrm{d}\gamma_3}(x_\alpha^m) = T_{I3}(x_\alpha^m)$, which means that we can use a suitable method of numerical integration, e.g., Runge–Kutta, from points x_α^m to points $\widetilde{x}_\alpha^m$.

2.2.2 Calculation of action functions with their lateral derivatives

Since calculating the action derivatives simultaneously with the action has turned out to be considerably more accurate than calculating the action alone, although in a slightly different problem (Klimeš, 1996), we prefer to apply it also to a system of Hamilton–Jacobi equations.

We assume that the values $S_I(x_\alpha^m)$ of action functions and their lateral derivatives $T_{I1}(x_\alpha^m)$, $T_{I2}(x_\alpha^m)$ along a given surface are known at given discrete points x_α^m situated at the given surface. We then calculate these values at corresponding points $\widetilde{x}_\alpha^m$ situated at the subsequent surface.

For known T_{I1} and T_{I2}, (16) represents the system of N nonlinear equations for N unknowns T_{I3}. By solving this system, we obtain derivatives T_{I3} of S_I along the path of integration at each point x_α^m.

We now define second–order action derivatives

$$T_{Iab} = S_{I,jk}\, t_a^j\, t_b^k \tag{17}$$

covariantly transformed to vectors t_a^j. We need to calculate derivatives T_{I13} and T_{I23} of T_{I1} and T_{I2} along the path of integration.

We multiply equations (5) by vectors t_1^i, t_2^i, t_3^i, insert (13), consider (17), and obtain equations

$$H^{I,Jj}\, \hat{t}_j^a\, T_{J,ab} + H^I_{,i}\, t_b^i = 0 \quad . \tag{18}$$

We define matrices c^{IJ1}, c^{IJ2} and c^{IJ3} by relation

$$C^{IJa} = H^{I,Jj}\, \hat{t}_j^a \quad . \tag{19}$$

Equations (18) then read

$$C^{IJa}\, T_{J,ab} + H^I_{,i}\, t_b^i = 0 \quad . \tag{20}$$

Equations (20) yield equations

$$\boxed{T_{I13} = -C_{IK3}\left(C^{KJ1}\, T_{J11} + C^{KJ2}\, T_{J12} + H^K_{,i}\, t_1^i\right)} \tag{21}$$

and

$$\boxed{T_{I23} = -C_{IK3}\left(C^{KJ1}\, T_{J12} + C^{KJ2}\, T_{J22} + H^K_{,i}\, t_2^i\right) \quad ,} \tag{22}$$

where C_{IJ3} denote the components of the matrix inverse to C^{IJ3},

$$C_{IJ3}\, C^{JK3} = \delta_I^K \quad . \tag{23}$$

We calculate lateral derivatives T_{I11}, T_{I12} and T_{I22} of T_{I1} and T_{I2} along the given surface by finite differences. Note that calculating lateral derivatives T_{I11}, T_{I12} and T_{I22} may represent a considerable problem in vicinities of caustics, where these derivatives may be infinitely large.

We then use equations (21) and (22) for calculating derivatives T_{I13} and T_{I23} from lateral derivatives T_{I11}, T_{I12} and T_{I22}.

We can thus calculate, for given $S_I(x_\alpha^m)$, $T_{I1}(x_\alpha^m)$ and $T_{I2}(x_\alpha^m)$, their derivatives

$$\frac{\mathrm{d}S_J}{\mathrm{d}\gamma_3}(x_\alpha^m) = T_{I3}(x_\alpha^m) \quad , \qquad \frac{\mathrm{d}T_{J1}}{\mathrm{d}\gamma_3}(x_\alpha^m) = T_{I13}(x_\alpha^m) \quad , \qquad \frac{\mathrm{d}T_{J2}}{\mathrm{d}\gamma_3}(x_\alpha^m) = T_{I23}(x_\alpha^m) \tag{24}$$

along the path of integration, which means that we can use a suitable method of numerical integration, e.g., Runge–Kutta, from points x_α^m to points $\widetilde{x}_\alpha^m$.

We calculate lateral derivatives $T_{I1}(x_\alpha^m)$ and $T_{I2}(x_\alpha^m)$ by numerical integration of equations (21) and (22). Actions $S_I(x_\alpha^m)$ are obtained by numerical quadrature of $T_{I3}(x_\alpha^m)$ resulting from equation (16). The lateral derivatives of actions $S_I(x_\alpha^m)$ then slowly but steadily become different from $T_{I1}(x_\alpha^m)$ and $T_{I2}(x_\alpha^m)$. In order to maintain a relation between $T_{I1}(x_\alpha^m)$, $T_{I2}(x_\alpha^m)$ and the lateral derivatives of $S_I(x_\alpha^m)$, we may apply modifications

$$T_{I1}(x_\alpha^m) \longrightarrow T_{I1}(x_\alpha^m) + q\left[T_{I1}^{\mathrm{FD}}(x_\alpha^m) - T_{I1}(x_\alpha^m)\right] \tag{25}$$

and

$$T_{I2}(x_\alpha^m) \longrightarrow T_{I2}(x_\alpha^m) + q\left[T_{I2}^{\mathrm{FD}}(x_\alpha^m) - T_{I2}(x_\alpha^m)\right] \tag{26}$$

with small coefficient q during each step of numerical integration. Here $T_{I1}^{\mathrm{FD}}(x_\alpha^m)$ and $T_{I2}^{\mathrm{FD}}(x_\alpha^m)$ are calculated from $S_I(x_\alpha^m)$ by finite differences.

The applicability of equations (16), (21) and (22) to the calculation of action depends on the relations between the directions of vectors t_1^j, t_2^j, t_3^j and the phase–space derivatives $H^{I,Jj}$ of Hamiltonian functions. The applicability of equations (16), (21) and (22) should further be studied.

2.3. Complex–valued eikonal equation for isotropic attenuating media

We express the complex–valued eikonal equation for complex–valued travel time $\tau(x^m)$ in isotropic attenuating media in form

$$\tau_{,i}\tau_{,i} - v^{-2} = 0 \quad . \tag{27}$$

It represents the system of 2 Hamilton–Jacobi equations for 2 real–valued actions

$$S_1 = \mathrm{Re}(\tau) \quad , \qquad S_2 = \mathrm{Im}(\tau) \quad . \tag{28}$$

Inserting

$$\tau = S_1 + \mathrm{i}S_2 \tag{29}$$

into (27), we may define two real–valued Hamiltonian functions

$$H^1 = \tfrac{1}{2}\left(S_{1,i}\,S_{1,i} - S_{2,i}\,S_{2,i}\right) - w^1 \tag{30}$$

and

$$H^2 = S_{1,i}\,S_{2,i} - w^2 \quad , \tag{31}$$

where

$$w^1 = \tfrac{1}{2}\mathrm{Re}(v^{-2}) \tag{32}$$

and

$$w^2 = \tfrac{1}{2}\mathrm{Im}(v^{-2}) \quad . \tag{33}$$

To calculate T_{13} and T_{23} from the lateral first–order derivatives T_{11}, T_{12} T_{21} and T_{22}, we insert (29) with (15) into (27), and obtain complex–valued quadratic equation

$$(T_{1a} + \mathrm{i}T_{2a})\, G^{ab} (T_{1a} + \mathrm{i}T_{2a}) - v^{-2} = 0 \tag{34}$$

for $T_{13} + \mathrm{i}T_{23}$, where

$$G^{ab} = \hat{t}_i^a \, \hat{t}_i^b \tag{35}$$

is the contravariant metric tensor corresponding to local basis vectors t_1^i, t_2^i and t_3^i.

The first–order phase–space derivatives of Hamiltonian functions (30) and (31) are

$$H^{1,1i} = S_{1,i} \quad , \tag{36}$$

$$H^{1,2i} = -S_{2,i} \quad , \tag{37}$$

$$H^{2,1i} = S_{2,i} \quad , \tag{38}$$

$$H^{2,2i} = S_{1,i} \quad , \tag{39}$$

$$H^1_{,i} = -w^1_{,i} \quad , \tag{40}$$

$$H^2_{,i} = -w^2_{,i} \quad . \tag{41}$$

Inserting (36)–(39) with (15) into (19), we arrive at

$$C^{11a} = C^{22a} = G^{ab}\, T_{1b} \tag{42}$$

and

$$C^{21a} = -C^{12a} = G^{ab}\, T_{2b} \quad . \tag{43}$$

After inversion of 2×2 matrix C^{IK3}, we have all quantities required in equations (21)–(22).

If we choose t_3^j close to the direction of $S_{1,i}$, coefficients $C^{111} = C^{221}$ and $C^{112} = C^{222}$ are small with respect to $C^{113} = C^{223}$. If gradient $S_{2,i}$ is small with respect to gradient $S_{1,i}$, coefficients $C^{12a} = -C^{21a}$ are small with respect to $C^{113} = C^{223}$.

2.4. Application to wavefront tracing

In wavefront tracing, the reference wavefronts and reference real–valued travel time τ_{ref} are calculated in the reference non–attenuating velocity model. The reference travel time and its derivatives are calculated with a good accuracy. In order to minimize the numerical errors, we recommend to numerically solve the system of two Hamilton–Jacobi equations for differences

$$\Delta\tau = \tau - \tau_{\mathrm{ref}} \tag{44}$$

of the complex–valued travel time from the reference travel time rather than solving the Hamilton–Jacobi equations for complex–valued travel time. This approach should also efficiently replace the spherical correction used by Klimeš (1996) in regions where the wavefront is curved considerably.

A question remains how to modify wavefronts in vicinities of caustics in order to obtain a reasonable system of surfaces for calculating the complex–valued travel time.

3. Numerical examples for a constant vertical velocity gradient

In the 1–D model with constant vertical velocity gradient, the real part of velocity increases linearly with depth. The 2-D model volume is represented by a vertical square. The ratio of the real part of velocity between top and bottom is 1:3, and the real part of velocity gradient is $-2\,\mathrm{s}^{-1}$. If we assume that the dimensions of the square are $1\,\mathrm{km}\times 1\,\mathrm{km}$, the real part of velocity is $1\,\mathrm{km\,s}^{-1}$ at the top and $3\,\mathrm{km\,s}^{-1}$ at the bottom. The point source is situated at the left–hand top corner of the square. The real–valued velocity model was used by Podvin & Lecomte (1991) to study the accuracy of their first–order grid travel–time tracing method, and also by Klimeš (1996).

In order to make coding the numerical solution of the system of two Hamilton–Jacobi equations for complex–valued travel time as simple as possible, we coded very primitive version, in which the system of surfaces for calculation of travel time is formed by vertical lines. One advantage of this primitive version is the possibility to test the behaviour of the numerical solution for large angles between the slowness vector and vector t_3^i.

Since this primitive version obviously cannot be applied in the vicinity of the point source, we calculate the complex–valued travel time in the right–hand half of the vertical square only. If we introduce horizontal coordinate x^1 extending from $x^1 = 0.000\,\mathrm{km}$ at the left–hand side of the square to $x^1 = 1.000\,\mathrm{km}$ at the right–hand side and vertical coordinate x^3 extending from $x^3 = -1.000\,\mathrm{km}$ at the bottom to $x^3 = 0.000\,\mathrm{km}$ at the top, the point source is located at $x^1 = 0.000\,\mathrm{km}$, $x^3 = 0.000\,\mathrm{km}$, and we calculate the complex–valued travel time from $x^1 = 0.500\,\mathrm{km}$ to $x^1 = 1.000\,\mathrm{km}$. The initial complex–valued travel time is calculated analytically along the vertical line situated at $x^1 = 0.500\,\mathrm{km}$. The spacing between subsequent vertical lines for calculation of travel time is $0.005\,\mathrm{km}$. We thus have 101 vertical lines between $x^1 = 0.500\,\mathrm{km}$ and $x^1 = 1.000\,\mathrm{km}$. We select 201 discrete points along each vertical line between $x^3 = -1.000\,\mathrm{km}$ and $x^3 = 0.000\,\mathrm{km}$.

In these coordinates, we choose

$$\begin{pmatrix} t_1^1 & t_3^1 \\ t_1^3 & t_3^3 \end{pmatrix} = \begin{pmatrix} 0 & 1 \\ 1 & 0 \end{pmatrix} \quad . \tag{45}$$

We then calculate four values

$$S_I(x_\alpha^m) \quad , \qquad T_{I1}(x_\alpha^m) = S_{I,3}(x_\alpha^m) \tag{46}$$

at each of 201 points along a vertical line. Along each vertical line, we calculate the lateral derivatives $T_{I1}^{\mathrm{FD}}(x_\alpha^m)$ and $T_{I11}(x_\alpha^m)$ of $S_I(x_\alpha^m)$ and $T_{I1}(x_\alpha^m)$ by simple finite differences from the 3 points nearest to x_α^m. Derivatives $T_{I3}(x_\alpha^m)$ and $T_{I13}(x_\alpha^m)$ of $S_I(x_\alpha^m)$ and $T_{I1}(x_\alpha^m)$ in the horizontal direction are calculated using equations (16) and (20). For stabilization (25), we use $q = 0.002$. We apply fourth–order Runge–Kutta subroutine `RKGS` to the numerical integration of 804 ordinary differential equations in the horizontal direction. We avoid halving the intervals between subsequent vertical lines.

We perform all calculations in single precision. We compare the numerical solution with the analytical solution in order to obtain the absolute travel–time errors of the numerical solution.

3.1. Analytical solution

We consider velocity model

$$v(x^k) = v_0 + b\,x^3 \tag{47}$$

with constant vertical velocity gradient b. The analytical expression for the two–point travel time reads (Červený, 2001, sec. 3.7.2.4)

$$\tau(x^k, x_0^l) = \pm b^{-1}\mathrm{arccosh}(1+\xi) \quad , \tag{48}$$

where

$$\xi = \frac{b^2\,|x|^2}{2\,v(x^k)\,v(x_0^l)} \tag{49}$$

with

$$|x| = \sqrt{(x^j - x_0^j)(x^j - x_0^j)} \quad . \tag{50}$$

We express equation (48) in more practical form

$$\tau(x^k, x_0^l) = \pm b^{-1}\ln\Big(1 + \xi + \sqrt{(2+\xi)\,\xi}\,\Big) \quad . \tag{51}$$

Equation (51) is also applicable to complex–valued velocity $v(x^k)$ and to complex–valued position x_0^k of the source.

We now calculate the first–order spatial derivatives

$$\tau_{,i}(x^k, x_0^l) = \frac{\partial\tau}{\partial\xi}\,\xi_{,i} \tag{52}$$

of travel time (51) with respect to x^i, We first differentiate (51) with respect to ξ,

$$\frac{\partial\tau}{\partial\xi} = \pm b^{-1}\Big(1+\xi+\sqrt{(2+\xi)\,\xi}\,\Big)^{-1}\Big(1+(1+\xi)/\sqrt{(2+\xi)\,\xi}\,\Big) = \pm b^{-1}\Big(\sqrt{(2+\xi)\,\xi}\,\Big)^{-1}. \tag{53}$$

We differentiate (49) with respect to x^i,

$$\xi_{,i} = \frac{b^2(x^i - x_0^i)}{v(x^k)\,v(x_0^l)} - \frac{b^3\,|x|^2}{2\,v^2(x^k)\,v(x_0^l)}\,\delta_3^i \quad , \tag{54}$$

which we convert to

$$\xi_{,i} = \frac{b^2}{v^2(x^k)\,v(x_0^l)}\,\left[v(x^k)\,(x^i - x_0^i) - \tfrac{1}{2}b\,|x|^2\delta_3^i\right] \quad . \tag{55}$$

For the first component, equation (55) reads

$$\xi_{,1} = \frac{b^2}{v^2(x^k)\,v(x_0^l)}\,v(x^k)\,(x^1 - x_0^1) \quad . \tag{56}$$

For the third component, equation (55) reads

$$\xi_{,3} = \frac{b^2}{v^2(x^k)\,v(x_0^l)}\,\tfrac{1}{2}[2v(x^k)\,(x^3 - x_0^3) - b\,|x|^2] \quad , \tag{57}$$

which can also be expressed as

$$\xi_{,3} = \frac{b^2}{v^2(x^k)\,v(x_0^l)}\,\tfrac{1}{2}\big\{[v(x^k) + v(x_0^k)]\,(x^3 - x_0^3) - b\,(x^1 - x_0^1)^2\big\} \quad . \tag{58}$$

We use equations (56) and (58) to calculate the first–order spatial derivatives (52) of complex–valued travel time. It is sufficient to calculate the expressions standing to the right of the first fractions in (56) and (58), and to normalize the obtained vector to $1/v(x^k)$

3.2. Point source in a complex–valued velocity model

We choose the complex–valued velocity of $(1 - \mathrm{i}0.05)\,\mathrm{km\,s^{-1}}$ at the top and $(3 - \mathrm{i}0.00)\,\mathrm{km\,s^{-1}}$ at the bottom. The quality factor is thus around $Q = 10$ (depending on the definition of Q) at the top and $Q = +\infty$ at the bottom. The constant vertical velocity gradient is $(-2 - \mathrm{i}0.05)\,\mathrm{s^{-1}}$.

We consider the point source located at $x^1 = 0.000\,\mathrm{km}$, $x^3 = 0.000\,\mathrm{km}$, and calculate analytically the initial complex–valued travel time along vertical line $x^1 = 0.500\,\mathrm{km}$.

We than calculate numerically the complex–valued travel time along other 100 vertical lines from $x^1 = 0.505\,\mathrm{km}$ to $x^1 = 1.000\,\mathrm{km}$, see Figures 1 and 2. We clearly observe that the wave is inhomogeneous, i.e., that the gradients of real and imaginary parts of travel time have different directions. We compare the numerical solution with the analytical solution in order to obtain the absolute travel–time errors of the numerical solution, see the captions of Figures 1 and 2.

3.3. Gaussian beam in a real–valued velocity model

We choose the real–valued velocity of $1\,\mathrm{km\,s^{-1}}$ at the top and $3\,\mathrm{km\,s^{-1}}$ at the bottom. The constant vertical velocity gradient is $-2\,\mathrm{s^{-1}}$.

We shift the point source to complex–valued position $x^1 = (0.000 + \mathrm{i}0.110)\,\mathrm{km}$, $x^3 = (0.000 - \mathrm{i}0.150)\,\mathrm{km}$. We calculate analytically the initial complex–valued travel time along vertical line $x^1 = 0.500\,\mathrm{km}$. This initial travel time corresponds to the strict Gaussian beam.

We than calculate numerically the complex–valued travel time of the strict Gaussian beam along other 100 vertical lines from $x^1 = 0.505\,\mathrm{km}$ to $x^1 = 1.000\,\mathrm{km}$, see Figures 3 and 4. Since the velocity is real–valued, the gradients of real and imaginary parts of travel time are mutually perpendicular. We compare the numerical solution with the analytical solution in order to obtain the absolute travel–time errors of the numerical solution, see the captions of Figures 3 and 4.

3.4. Gaussian beam in a complex–valued velocity model

We choose the complex–valued velocity of $(1 - \mathrm{i}0.05)\,\mathrm{km\,s^{-1}}$ at the top and $(3 - \mathrm{i}0.00)\,\mathrm{km\,s^{-1}}$ at the bottom. The quality factor is thus around $Q = 10$ at the top and $Q = +\infty$ at the bottom. The constant vertical velocity gradient is $(-2 - \mathrm{i}0.05)\,\mathrm{s^{-1}}$.

We leave the point source at complex–valued position $x^1 = (0.000 + \mathrm{i}0.110)\,\mathrm{km}$, $x^3 = (0.000 - \mathrm{i}0.150)\,\mathrm{km}$. We calculate analytically the initial complex–valued travel time along vertical line $x^1 = 0.500\,\mathrm{km}$. This initial travel time corresponds to the strict Gaussian beam in the attenuating medium.

We than calculate numerically the complex–valued travel time of the strict Gaussian beam along other 100 vertical lines from $x^1 = 0.505\,\mathrm{km}$ to $x^1 = 1.000\,\mathrm{km}$, see Figures 5 and 6. If we compare Figure 5 with Figure 4, we clearly observe the shift of the envelope of the Gaussian beam caused by the heterogeneous attenuation. We compare the numerical solution with the analytical solution in order to obtain the absolute travel–time errors of the numerical solution, see the captions of Figures 5 and 6.

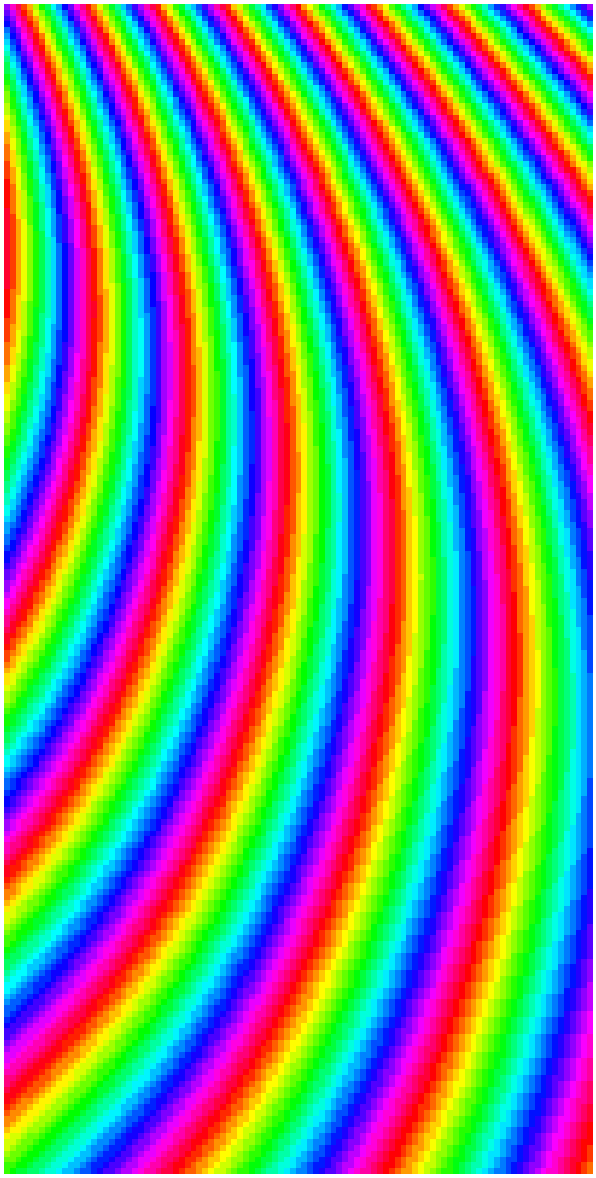

Figure 1. The real part of travel time corresponding to the point source located at $x^1 = 0.000\,\mathrm{km}$, $x^3 = 0.000\,\mathrm{km}$ in the complex–valued velocity model with velocity $(1 - \mathrm{i}0.05)\,\mathrm{km\,s^{-1}}$ at the top and $(3 - \mathrm{i}0.00)\,\mathrm{km\,s^{-1}}$ at the bottom. The values of the real part of travel time range from 0.440 s to 0.880 s. The colour circle corresponds to the time increment of 0.050 s. The yellow colour corresponds to values 0.450 s, 0.500 s, 0.550 s, etc. The maximum absolute error of the numerical solution is 1.3×10^{-6}s.

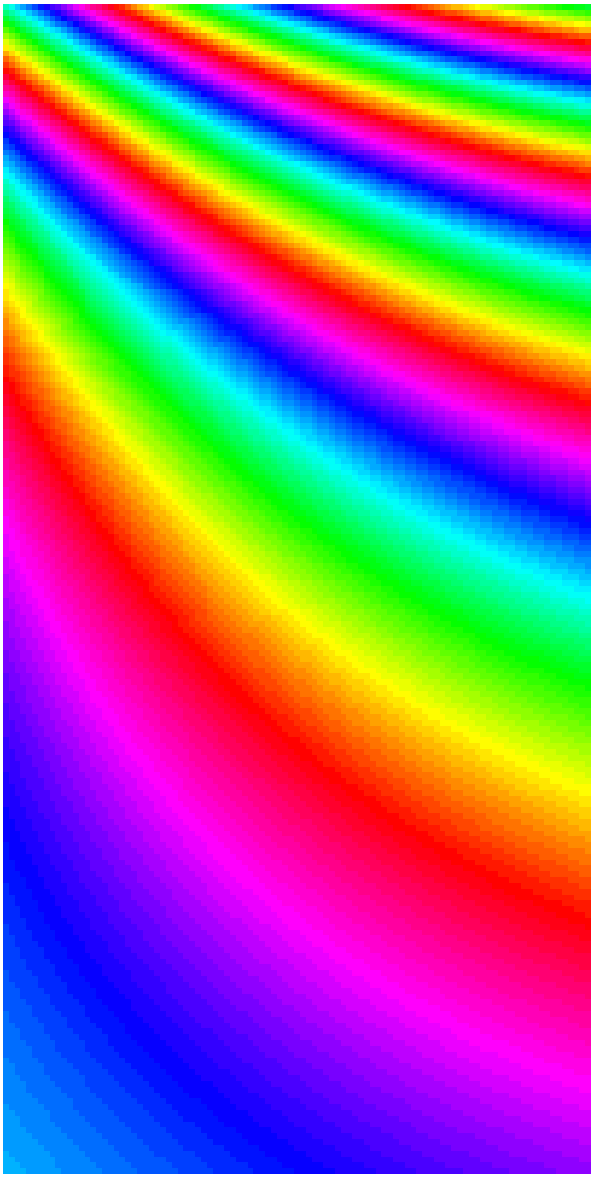

Figure 2. The imaginary part of travel time corresponding to the point source located at $x^1 = 0.000\,\mathrm{km}$, $x^3 = 0.000\,\mathrm{km}$ in the complex–valued velocity model with velocity $(1 - \mathrm{i}0.05)\,\mathrm{km\,s^{-1}}$ at the top and $(3 - \mathrm{i}0.00)\,\mathrm{km\,s^{-1}}$ at the bottom. The values of the imaginary part of travel time range from 0.012 s to 0.031 s. The colour circle corresponds to the time increment of 0.005 s. The yellow colour corresponds to values 0.015 s, 0.020 s, 0.025 s and 0.030 s. The maximum absolute error of the numerical solution is 0.6×10^{-6}s.

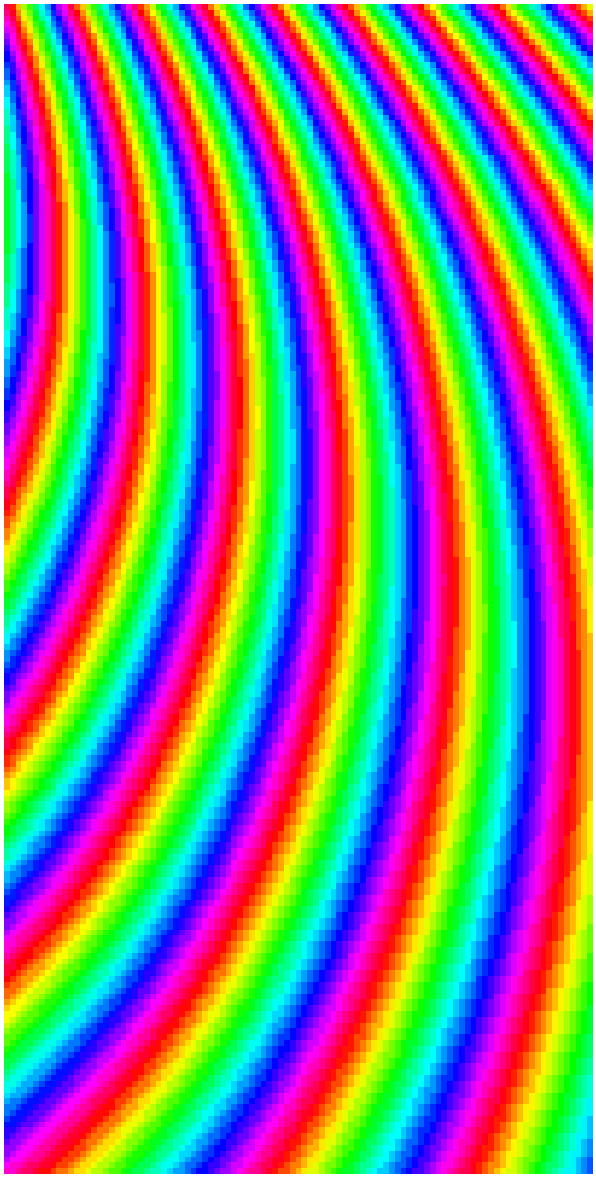

Figure 3. The real part of travel time of the strict Gaussian beam corresponding to the point source located at complex–valued position $x^1 = (0.000 + \mathrm{i}0.110)\,\mathrm{km}$, $x^3 = (0.000 - \mathrm{i}0.150)\,\mathrm{km}$ in the real–valued velocity model with velocity $1\,\mathrm{km\,s^{-1}}$ at the top and $3\,\mathrm{km\,s^{-1}}$ at the bottom. The values of the real part of travel time range from 0.410 s to 0.851 s. The colour circle corresponds to the time increment of 0.050 s. The yellow colour corresponds to values 0.450 s, 0.500 s, 0.550 s, etc. The maximum absolute error of the numerical solution is 2.4×10^{-6}s.

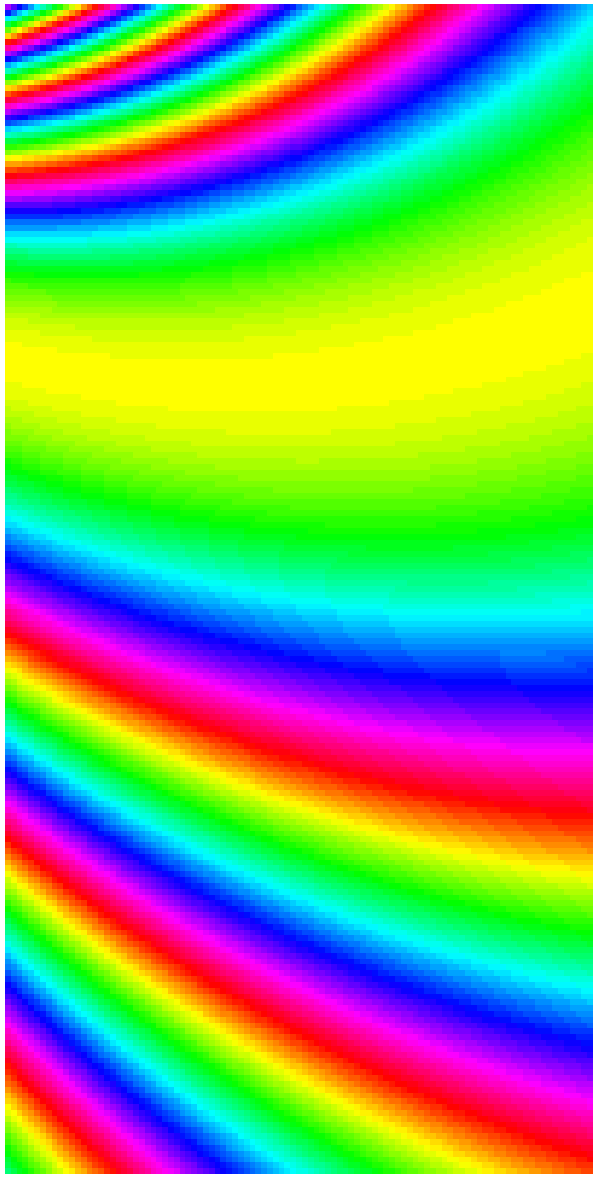

Figure 4. The imaginary part of travel time of the strict Gaussian beam corresponding to the point source located at complex–valued position $x^1 = (0.000 + \mathrm{i}0.110)\,\mathrm{km}$, $x^3 = (0.000 - \mathrm{i}0.150)\,\mathrm{km}$ in the real–valued velocity model with velocity $1\,\mathrm{km\,s^{-1}}$ at the top and $3\,\mathrm{km\,s^{-1}}$ at the bottom. The values of the imaginary part of travel time range from -0.182 s to -0.164 s, where the minimum value of -0.182 s corresponds to the axial ray of the Gaussian beam. The values of the imaginary part of travel time rescaled to the value at the axial ray range from 0.000 s to 0.019 s. The colour circle corresponds to the time increment of 0.005 s. The yellow colour corresponds to rescaled values 0.000 s, 0.005 s, 0.010 s and 0.015 s. The maximum absolute error of the numerical solution is 2.4×10^{-6}s.

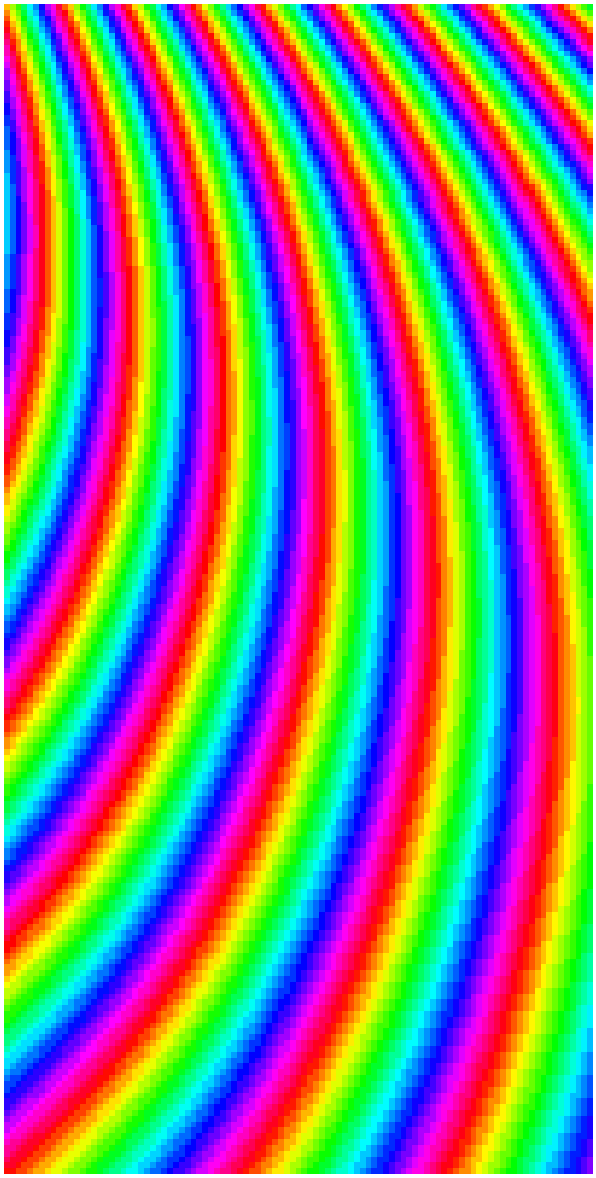

Figure 5. The real part of travel time of the strict Gaussian beam corresponding to the point source located at complex–valued position $x^1 = (0.000 + \mathrm{i}0.110)\,\mathrm{km}$, $x^3 = (0.000 - \mathrm{i}0.150)\,\mathrm{km}$ in the complex–valued velocity model with velocity $(1 - \mathrm{i}0.05)\,\mathrm{km\,s^{-1}}$ at the top and $(3 - \mathrm{i}0.00)\,\mathrm{km\,s^{-1}}$ at the bottom. The values of the real part of travel time range from 0.418 s to 0.860 s. The colour circle corresponds to the time increment of 0.050 s. The yellow colour corresponds to values 0.450 s, 0.500 s, 0.550 s, etc. The maximum absolute error of the numerical solution is 7.6×10^{-6}s.

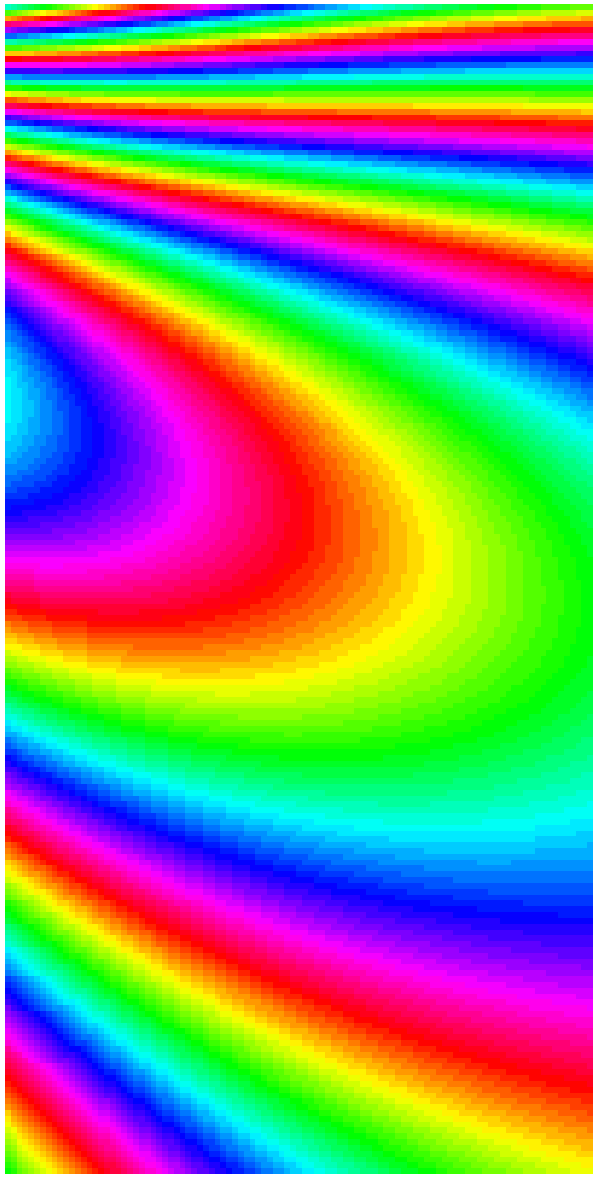

Figure 6. The imaginary part of travel time of the strict Gaussian beam corresponding to the point source located at complex–valued position $x^1 = (0.000 + \mathrm{i}0.110)\,\mathrm{km}$, $x^3 = (0.000 - \mathrm{i}0.150)\,\mathrm{km}$ in the complex–valued velocity model with velocity $(1 - \mathrm{i}0.05)\,\mathrm{km\,s^{-1}}$ at the top and $(3 - \mathrm{i}0.00)\,\mathrm{km\,s^{-1}}$ at the bottom. The values of the imaginary part of travel time range from -0.171 s to -0.146 s. The values of the imaginary part of travel time rescaled to the value of -0.182 s at the axial ray in the non–attenuating medium (Figure 4) range from 0.012 s to 0.036 s. The colour circle corresponds to the time increment of 0.005 s. The yellow colour corresponds to rescaled values 0.015 s, 0.020 s, ..., 0.035 s. The maximum absolute error of the numerical solution is 6.7×10^{-6}s.

4. Conclusions

In real space, the eikonal equation for complex–valued travel time represents the system of two Hamilton–Jacobi equations for the real and imaginary parts of the complex–valued travel time. The solution of this system of Hamilton–Jacobi equations does not propagate along rays, and has to be solved by more global numerical methods.

We have proposed to consider a system of surfaces and to calculate the complex–valued travel time from one surface to the subsequent surface numerically. This method may be suitable for application to wavefront tracing (Vinje, Iversen & Gjøystdal, 1993; Vinje et al., 1996), but poses a problem how to modify wavefronts in vicinities of caustics in order to obtain a reasonable system of surfaces for calculating the complex–valued travel time.

The system of surfaces for calculating the complex–valued travel time should respect the multi–valued nature of travel time, which implies that the selection of the surfaces will constitute a very difficult task.

Calculating the lateral derivatives of the complex–valued travel time along individual surfaces may represent a considerable problem in vicinities of caustics, where the second–order derivatives of the complex–valued travel time are very large.

The numerical solution of the system of two Hamilton–Jacobi equations for complex–valued travel time has been found very unstable and very sensitive to numerical parameters. On the other hand, we tested the numerical solution in a considerably suboptimal configuration with respect to the direction of propagation.

The solution of the system of Hamilton–Jacobi equations for complex–valued travel time will require to design new numerical algorithms, to study the stability and accuracy of these algorithms, and to estimate the propagation of numerical errors in these algorithms.

Acknowledgements

The author is indebted to Vlastislav Červený for many discussions and for offering the paper by Suchy (1972).

The research has been supported by the Grant Agency of the Czech Republic under contract 205/07/0032, by the Ministry of Education of the Czech Republic within research project MSM0021620860, and by the members of the consortium "Seismic Waves in Complex 3–D Structures" (see "http://sw3d.cz").

References

Červený, V. (2001): *Seismic Ray Theory.* Cambridge Univ. Press, Cambridge.

Hamilton, W.R. (1837): Third supplement to an essay on the theory of systems of rays. *Trans. Roy. Irish Acad.*, **17**, 1–144.

Klimeš, L. (1996): Grid travel–time tracing: second–order method for the first arrivals in smooth media. *Pure appl. Geophys.*, **148**, 539–563.

Podvin, P. & Lecomte, I. (1991): Finite difference computation of traveltimes in very contrasted velocity models: a massively parallel approach and its associated tools. *Geophys. J. int.*, **105**, 271–284.

Suchy, K. (1972): Ray tracing in an anisotropic absorbing medium. *J. Plasma Phys.*, **8**, 53–65.

Vidale, J.E. (1988): Finite–difference calculation of travel times. *Bull. Seismol. Soc. Amer.*, **78**, 2062–2076.

Vinje, V., Iversen, E. & Gjøystdal, H. (1993): Traveltime and amplitude estimation using wavefront construction. *Geophysics*, **58**, 1157–1166.

Vinje, V., Iversen, E., Åstebøl, K. & Gjøystdal, H. (1996): Estimation of multivalued arrivals in 3D models using wavefront construction — Part I. *Geophys. Prospecting*, **44**, 819–842.